JOM, Vol. 67, No. 7, 2015
DOI: 10.1007/s11837-015-1401-0

Process Optimization of Seed Precipitation Tank with Multiple Impellers Using Computational Fluid Dynamics

HONG-LIANG ZHAO,[1,2] CHAO LV,[2] YAN LIU,[2,3] and TING-AN ZHANG[2]

1.—Beijing Key Laboratory of Green Recycling and Extraction of Metal, University of Science & Technology Beijing, Beijing 100083, People's Republic of China. 2.—Key Laboratory of Ecological Utilization of Multi-Metal Intergrown Ores of Ministry of Education & School of Materials and Metallurgy, Northeastern University, Shenyang 100819, People's Republic of China. 3.—e-mail: shanqibao2000@163.com

The complex fluid flow in a large-scale tank stirred with multiple Ekato Intermig impellers used in the seed precipitation process was numerically analyzed by the computational fluid dynamics method. The flow field, liquid–solid mixing, and power consumption were simulated by adopting the Eulerian granular multiphase model and standard k–ε turbulence model. A steady multiple reference frame approach was used to represent impeller rotation. The simulated results showed that the five-stage multiple Intermig impeller coupled with sloped baffles could generate circulation loops in axial, which is good for solid uniform mixing. The fluid is overmixed under the current industrial condition. Compared with the current process conditions, a three-stage impeller with L/D of 1.25 not only could meet the industrial requirements, but also more than 20% power could be saved. The results have important implications for reliable design and optimal performance for industry.

INTRODUCTION

In recent years, a type of large-scale tank stirred with multiple Intermig impellers has been widely used in the seed precipitation process of the Bayer method to produce aluminum oxide in China; examples of such technologies are located at the Shanxi aluminum plant and the Guizhou aluminum plant. In 2000, Shenyang Aluminum & Magnesium Engineering & Research Institute (SAMI) of China designed a new type of mechanically agitated tank with sloped baffles and an improved Intermig impeller.[1] The industrial practice indicated that the fluid mixing and $Al(OH)_3$ particles suspension were obviously improved in the new tank. Especially, the power consumption was greatly reduced compared with the tank stirred with a pitched-blade impeller. However, the process technology of this new tank is unknown, and little information, such as the mixing characteristics, flow field or power consumption, has been well acquainted. So it is necessary to study systemically the mixing performance of this new type of large-scale tank, which has important meaning for reliable design and optimal performance in industry.

Currently, many studies focused on the fluid characteristic in the tank stirred with multiple impellers. Dohi et al.[2] experimentally analyzed the solid-suspension characteristics in gas–liquid–solid three-phase stirred tanks with three-stage impellers of two four-pitched blade down-flow disk turbines and one Pfaudler type impeller, which provided good gas dispersion and accomplished off-bottom suspension. Magelli et al.[3] investigated the solid distribution for solid–liquid suspensions in a vessel stirred with four-stage six-bladed Rushton turbines experimentally. The average solid concentrations were measured by using an optical technique, and the solid profiles were well modeled by the one-dimensional sedimentation-dispersion model. Kasat and Pandit[4] studied the mixing time in a multiple impeller-agitated reactor by a conductivity measurement technique and explained the experimental results on the basis of the liquid-phase axial dispersion coefficient and cell residence time. Aubin and Xuereb[5] investigated hydrodynamics and mixing performance in highly viscous system stirred with the multiple Intermig impellers using computational fluid dynamics (CFD). The relationship between the fluid exchange and the impeller

(Published online April 17, 2015)

configuration and Reynolds number were obtained. However, most of the current research was conducted at the laboratory scale, and few of these investigations involved the high solid content slurry system and multiple Intermig impellers.

Previous works have investigated a laboratory-scale tank stirred with single Intermig impeller using the experiment and simulation method by Professor Zhang's group.[6,7] In this work, the industrial large-scale seed precipitation tank is studied by the CFD method. The Eulerian granular multiphase (EGM) model and standard k–ε turbulence model are adopted to describe the liquid–solid two phases flow behavior. The influence of separation distance of each impeller (L) on the flow field, liquid–solid mixing, and power consumption is numerically simulated based on the mathematical models verified by experiments in the laboratory-scale research.

TANK GEOMETRY

The seed precipitation tank simulated in this work is a cylindrical tank with a flat bottom. Two specially sloped baffles and a feed pipe were installed in the tank with a diameter (T) of 14 m and a height (H) of 29.5 m. The diameters of the inlet and outlet were both 0.7 m. The tank was equipped with five-stage Intermig impellers with 90° angles to each other in current industrial production. The upper four impellers are original structures, and the lowest one is improved in lengthening the outer blades. The diameter of upper impellers (D_u) is $0.6T$ and of the lowest (D_l) one is $0.714T$. The lowest impeller is set very close to the tank bottom and the off-bottom clearance (C) is $0.026T$. In this work, five cases have considered that the number of the impellers is changed from 5 to 2 according to the different separation distance of each impeller (L/D_u = 0.7–2). The impeller rotational speed is 4.8 r/min which is consistent with industrial conditions. The geometry model of the seed precipitation tank is shown in Fig. 1.

Figure 2 shows the structures of the upper original and lowest improved Intermig impellers. The Intermig impeller has two parts, the inner pitched blade and the outer double blades, and it is an interference multistage counter-flow impeller. The inner and outer blades are arranged in a staggered position with an opposing blade angle of 60°. The inner blade has 30° downward to the horizontal, and the outer blades are with a sloped angle of 30°. Compared with the original impeller (Fig. 2a), the improved one (Fig. 2b) is lengthened on one of the outer blade.

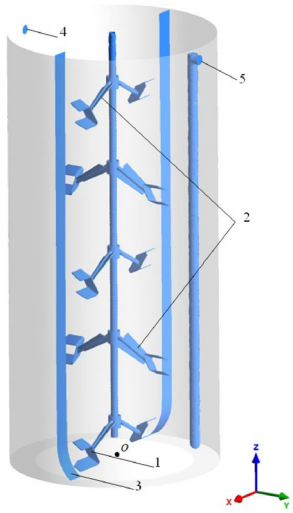

Fig. 1. Geometry of the seed precipitation tank: 1—lowest improved Intermig impeller, 2—upper original Intermig impellers, 3—sloped baffles, 4—material inlet, and 5—feed-pipe (material outlet).

SIMULATION METHOD

Governing Equations

The numerical simulation in the seed precipitation tank has been performed using an EGM model and a standard k–ε turbulence model.[8,9] The mass transfer, lift force and virtual mass force are not considered. The steady-state continuity and momentum equations are solved and for liquid phase are given below:

$$\nabla \cdot (\alpha_l \rho_l \vec{v}_l) = 0 \tag{1}$$

$$\nabla \cdot (\alpha_l \rho_l \vec{v}_l \vec{v}_l) = -\alpha_l \nabla p + \nabla \cdot \bar{\bar{\tau}}_l + \alpha_l \rho_l \vec{g} + \vec{F}_l + K_{sl}(\vec{v}_s - \vec{v}_l) \tag{2}$$

The continuity and momentum equations for solid phase are given below:

$$\nabla \cdot (\alpha_s \rho_s \vec{v}_s) = 0 \tag{3}$$

$$\nabla \cdot (\alpha_s \rho_s \vec{v}_s \vec{v}_s) = -\alpha_s \nabla p + \nabla \cdot \bar{\bar{\tau}}_s + \alpha_s \rho_s \vec{g} + \vec{F}_s + K_{ls}(\vec{v}_l - \vec{v}_s) \tag{4}$$

where $\bar{\bar{\tau}}_{l,s}$ is the phase stress–strain tensor that is computed by viscosity and Reynolds stress:

$$\bar{\bar{\tau}}_{l,s} = \alpha_{l,s}\mu_{l,s}\left[\left(\nabla \vec{v}_{l,s} + \nabla \vec{v}_{l,s}^{T}\right) - \frac{2}{3} I \nabla \cdot \vec{v}_{l,s}\right] \tag{5}$$

The volume fractions of liquid and solid phases in each calculated cell are normalized:

$$\alpha_l + \alpha_s = 1 \tag{6}$$

The momentum exchange coefficient is computed by the Gidaspow model,[10] which is usually selected in a high solid hold-up system.

When $\alpha_l > 0.8$, the liquid–solid exchange coefficient K_{ls} is of the following form:

(a) (b)

Fig. 2. Geometry of the Intermig impellers: (a) structure of upper impeller and (b) structure of lowest impeller.

$$K_{\mathrm{ls}} = K_{\mathrm{sl}} = \frac{3}{4} C_D \frac{\alpha_{\mathrm{s}} \alpha_{\mathrm{l}} \rho_{\mathrm{l}} \left| \vec{v}_{\mathrm{s}} - \vec{v}_{\mathrm{l}} \right|}{d_{\mathrm{s}}} \alpha_{\mathrm{l}}^{-2.65} \tag{7}$$

where C_{D} is the drag coefficient computed by:

$$C_{\mathrm{D}} = \frac{24}{\alpha_{\mathrm{l}} Re_{\mathrm{s}}} \left[1 + 0.15 (\alpha_{\mathrm{l}} Re_{\mathrm{s}})^{0.687} \right] \tag{8}$$

where Re_{s} is the relative Reynolds number computed by:

$$Re_{\mathrm{s}} = \frac{\rho_{\mathrm{l}} d_{\mathrm{s}} \left| \vec{v}_{\mathrm{s}} - \vec{v}_{\mathrm{l}} \right|}{\mu_{\mathrm{l}}} \tag{9}$$

When $\alpha_{\mathrm{l}} < 0.8$, K_{ls} is of the following form:

$$K_{\mathrm{ls}} = K_{\mathrm{sl}} = 150 \frac{\alpha_{\mathrm{s}} (1 - \alpha_{\mathrm{l}}) \mu_{\mathrm{l}}}{\alpha_{\mathrm{l}} d_{\mathrm{s}}^2} + 1.75 \frac{\alpha_{\mathrm{l}} \rho_{\mathrm{s}} \left| \vec{v}_{\mathrm{s}} - \vec{v}_{\mathrm{l}} \right|}{d_{\mathrm{s}}} \tag{10}$$

In the mixture standard k–ε turbulence model, both solid and liquid phases are assumed to share the same values of k and ε. The governing equations for turbulent kinetic energy k and turbulent energy dissipation rate ε are listed below:

$$\nabla \left(\rho \vec{v} k - \left(\frac{\mu_{\mathrm{t}}}{\sigma_{\mathrm{k}}} \right) \nabla k \right) = \alpha_{\mathrm{l}} (G_{\mathrm{l}} - \rho_{\mathrm{l}} \varepsilon) + \alpha_{\mathrm{s}} (G_{\mathrm{s}} - \rho_{\mathrm{s}} \varepsilon) \tag{11}$$

$$\nabla \left(\rho \vec{v} \varepsilon - \left(\frac{\mu_{\mathrm{t}}}{\sigma_{\varepsilon}} \right) \nabla \varepsilon \right) = \alpha_{\mathrm{l}} (C_1 G_{\mathrm{l}} - C_2 \rho_{\mathrm{l}} \varepsilon) \frac{\varepsilon}{k} + \alpha_{\mathrm{s}} (C_1 G_{\mathrm{s}} - C_2 \rho_{\mathrm{s}} \varepsilon) \frac{\varepsilon}{k} \tag{12}$$

where the mixture density ρ and velocity $\vec{v}$ are computed by:

$$\rho = \alpha_{\mathrm{l}} \rho_{\mathrm{l}} + \alpha_{\mathrm{s}} \rho_{\mathrm{s}} \tag{13}$$

and

$$\vec{v} = \frac{1}{\rho} (\alpha_{\mathrm{l}} \rho_{\mathrm{l}} \vec{v}_{\mathrm{l}} + \alpha_{\mathrm{s}} \rho_{\mathrm{s}} \vec{v}_{\mathrm{s}}) \tag{14}$$

μ_t is the turbulent viscosity computed by:

$$\mu_{\mathrm{t}} = \alpha_{\mathrm{l}} \mu_{\mathrm{tl}} + \alpha_{\mathrm{s}} \mu_{\mathrm{ts}} = \rho C_{\mu} \frac{k^2}{\varepsilon} \tag{15}$$

$G_{\mathrm{l,s}}$ is the generation of turbulence kinetic energy contributed by the mean velocity gradients:

$$G_{\mathrm{l,s}} = \frac{1}{2} \mu_{\mathrm{t(l,s)}} \left(\nabla \vec{v}_{\mathrm{l,s}} + \left(\nabla \vec{v}_{\mathrm{l,s}} \right)^{\mathrm{T}} \right)^2 \tag{16}$$

The parameters in the k–ε model are maintained as:

$$C_{\mu} = 0.09, C_1 = 1.44, C_2 = 1.92, \sigma_k = 1.0, \sigma_z = 1.3.$$

Boundary Conditions and Numerical Methods

In the computational model, the thickness of baffles is ignored and all the solid walls are treated as nonslip boundaries with standard wall functions. A steady multiple reference frame (MRF) method[11] is used, which simulates the impeller rotation. The free liquid surface is treated without flux and stress. The velocity inlet (with a flow rate of 0.7 m/s) and pressure outlet are used, which is the same as industrial conditions. The $NaAlO_2$ and $Al(OH)_3$ particles are used as liquid and solid phases, respectively, and the material properties are listed in Table I.

The Navier–Stokes equations are solved using a finite-volume method via a pressure–velocity-coupled SIMPLE algorithm. The governing equations are differenced by a second-upwind scheme and all the residuals are converged to 10^{-5}.

Mesh Model

Three-dimensional tetrahedral meshes are used to model the whole tank, and it is locally refined in rotational domain and around the baffles. A preliminary mesh convergence study was carried out to ensure the solution is mesh independent. Figure 3 shows the mesh model of seed precipitation tank stirred with multiple Intermig impellers.

RESULTS AND DISCUSSION

Model Verification

Mesh Independence

In this study, three grid sizes of 400,000, 800,000 and 1,600,000 cells were considered to investigate

Table I. Properties of liquid and solid

Material	$NaAlO_2$ solution	$Al(OH)_3$ particle
Density (kg/m^3)	1330	2430
Viscosity (Pa s)	0.007	–
Solid holdup (g/L)	–	800
Diameter (μm)	–	100

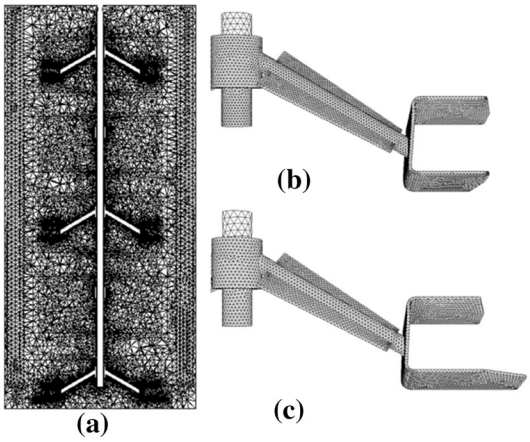

Fig. 3. Mesh model: (a) tank, (b) upper impeller, and (c) lowest impeller.

the effect of grid size on velocity and solid holdup distribution. The predicted results using different grids are listed in Figs. 4 and 5, respectively. The differences of velocity and solid holdup distributions in the axial (z) and radial (r) directions were found to be very small (~5%), with 800,000 and 1,600,000 cells. When adopting 400,000 cells, the differences of velocity and solid holdup increase greatly. Based on these results, all the subsequent simulations were carried out with approximately 800,000–1,200,000 computational cells.

Experimental Verification

The laboratory-scale experiments were carried out in a cold-water model stirred with double Intermig impellers. The tank has a diameter of 425 mm and a liquid surface height of 600 mm. The diameter ratio of the lower impeller to the tank is 0.714 and that of the upper one impeller to the tank is 0.6. A fiber-optic probe[12] is used to measure the concentration of the local solids. The average solid concentration in the entire tank is 800 g/L (c_{avg}).

Figure 6 exhibits the simulated and experimental results of the tank stirred with double impellers. Three impeller separation distances are investigated. When L/D = 0.5, the solid concentration difference is relatively higher because of the heterogeneous distribution of the stirred kinetic energy. When increasing L/D to 1 and 1.5, more uniform distribution of solid concentration could be obtained in the entire tank. Multiple Intermig impellers are suggested to be used with large impeller separation distances. The experimental and simulated results with double impellers show a good agreement. Based on the preceding analysis, the verified mathematical model is adopted to all the simulations of large-scale models.

Flow Field

Figure 7 shows the flow field generated by different stage impellers. From Fig. 7a, the secondary flows generated by the impeller at each stage superpose together to form two main circulation loops, which is good for axial mixing of fluids in the entire tank. With the increase of L/D, the connection of circulation loops between each impeller becomes weaker. At L/D = 1.25 (Fig. 7c), the secondary loops in each stage are close to the state of just connection. However, with such complex three-dimensional (3-D) flows, it is difficult to quantify whether the loops are well connected via the analysis of the two-dimensional data and to interpret whether the axial mixing is adequate. With a further increase in L/D, the circulation loops seem to be segregated, and it is almost entirely isolated at L/D = 2 (Fig. 7e); the loops have minimal exchange with each other.

To further investigate the fluid-mixing characteristics, the 3-D streamlines generated by lowest impeller with different L/D (colored by liquid velocity) were drawn (shown in Fig. 8). The fluids rotate fast around the each impeller, and the fluids velocity is relatively low for axial convection. For L/D = 0.7 (Fig. 8a), it can be seen that the fluids could be pumped from the lowest impeller to the top region and are mixed well into the entire tank. As the L/D increases (Fig. 8b and c), less impeller could ensure the fluid exchange between each impeller, although it seems to be slightly weaker. At L/D = 1.5 (Fig. 8d), little fluids stirred by lowest impeller could move to the upmost stage. Very poor fluid exchange occurs between the upper two impellers. With a further increase of L/D (Fig. 8e), the circulation loop generated by each impeller is entirely isolated and has minimal exchange between the lower and upper parts of the tank.

Solid Distribution

The solid volume fraction distribution at y = 0 section and on the bottom with different L/D are showed in Fig. 9. The solids distribute the most uniformly with five-stage impellers, which caused by intense interaction between each impeller. With the increasing of L/D, the solid concentration gradient in the entire tank becomes larger, especially in the top one-quarter region of the tank due to the lower stirring kinetic energy for mixing with less impeller. From the bottom, the solid holdup is relatively higher near the tank wall and at the center. Compared with L/D = 1, the solids distribute with a higher gradient at L/D = 0.7; because of that, the fluid is overmixed at a low impeller-separation

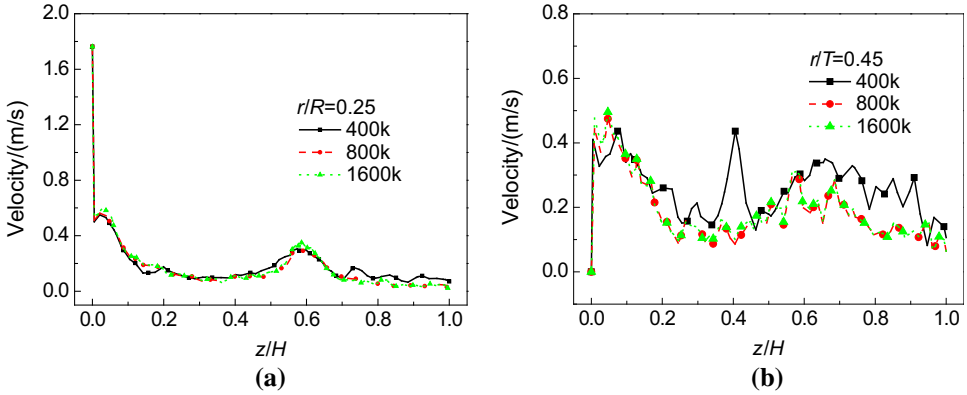

Fig. 4. Velocity distributions at different grid sizes: (a) r/T = 0.25 and (b) r/T = 0.45.

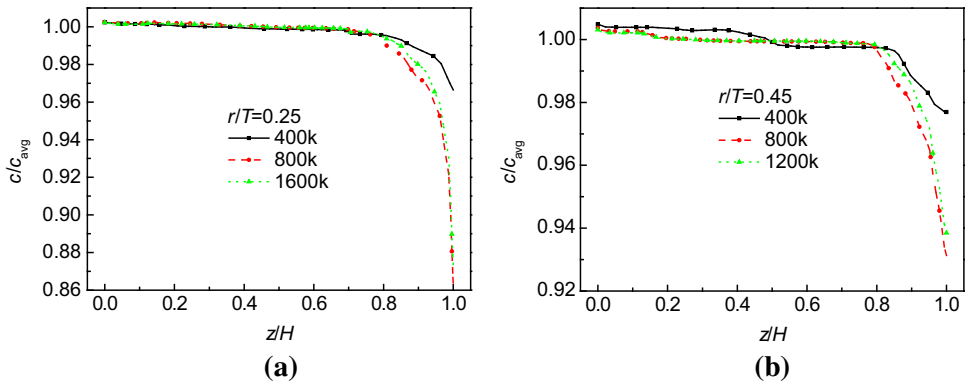

Fig. 5. Solid holdup at different grid sizes: (a) r/T = 0.25 and (b) r/T = 0.45.

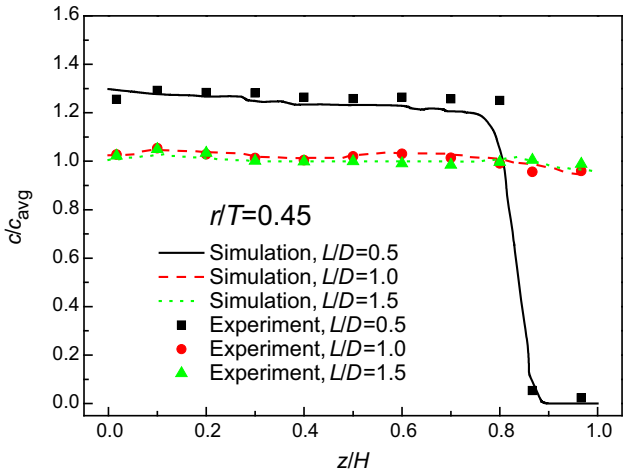

Fig. 6. Solids holdup comparison between experiment and simulation with double impellers at 250 r/min.

distance. With a further increase of L/D, the stirring for the second-stage impeller exerted on the bottom becomes weaker, so the solid profile changes little on the tank bottom.

Figure 10 shows the maximum relative solid volume fraction around each stage impeller with different L/D. When L/D = 0.7, because of overmixing around the bottom, more solid particles pump to the second-stage region; the maximum of solid concentration exists near the axis this second-stage region. When increasing L/D, the position with maximum solid concentration transfers to the lowest stage region; meanwhile, the concentration difference in the rotational region becomes smaller.

These results suggest that the fluid, especially on the tank bottom, is overmixed under the current industrial conditions (L/D = 0.7). This result indicates that the solid could still mix well with less impeller.

Mixing Performance

The following two indicators have been used to estimate the mixing effect in industry.

(1) The concentration difference between any two positions in the whole tank is less than 3% to 5%.

$$\Delta c_{\max} = (c_{\max} - c_{\min})/c_{\text{avg}} < 3\% \text{ to } 5\% \qquad (17)$$

(2) The concentration increment in the feed pipe is less than 0.6%.

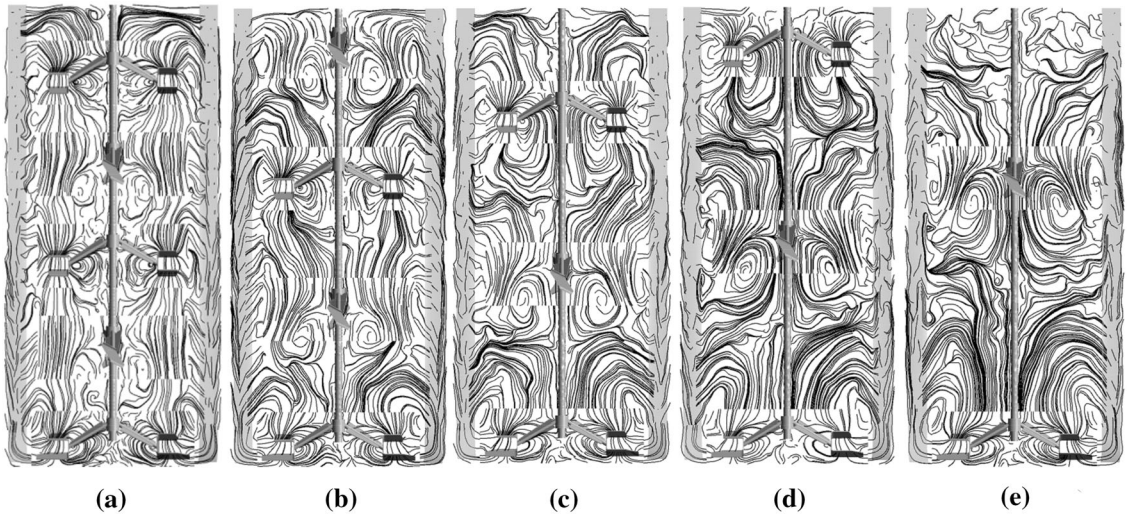

Fig. 7. Liquid streamlines with different L/D at $Y = 0$ section: (a) five-stage ($L/D = 0.7$), (b) four-stage ($L/D = 1$), (c) three-stage ($L/D = 1.25$), (d) three-stage ($L/D = 1.5$), and (e) two-stage ($L/D = 2$).

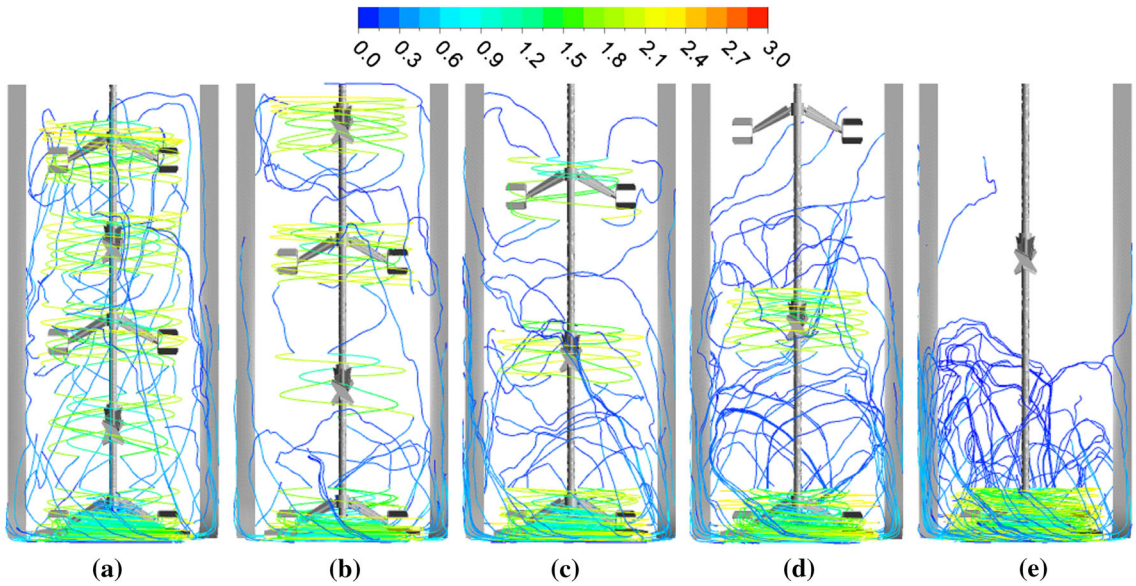

Fig. 8. Three-dimensional streamlines generated by lowest impeller with different L/D (color map shows velocity magnitude, m/s): (a) five-stage ($L/D = 0.7$), (b) four-stage ($L/D = 1$), (c) three-stage ($L/D = 1.25$), (d) three-stage ($L/D = 1.5$), and (e) two-stage ($L/D = 2$).

$$\Delta c_{\text{inc}} = \left(c - c_{\text{avg}}\right)/c_{\text{avg}} < 0.6\% \tag{18}$$

Figure 11 shows the maximum concentration difference in the entire tank with different L/D. It can be observed that the maximum concentration difference is increased with increasing L/D. Based on the previous analysis, overmixing of five-stage impeller causes a higher concentration distribution in the rotational region. However, the solids mix more uniformly near the surface. So the maximal concentration difference is the lowest. Using only three-stage impeller with L/D of 1.25 can meet the requirement of the first indicator ($\Delta c_{\max} < 5\%$).

Figure 12 shows the axial distribution of concentration increment in the feed pipe with different L/D. The concentration increment in the feed pipe is less than 0.6% in all the five cases. The concentration increases the least with a three-stage impeller of $L/D = 1.5$. But because of relatively poor axial mixing, the three-stage impeller and $L/D = 1.5$ is not the best options for industrial production.

Power Consumption

The power consumptions could be calculated by:

$$P = M\omega = 2\pi NM/60 \tag{19}$$

where M is the torque obtained by the surface integral of each impeller.

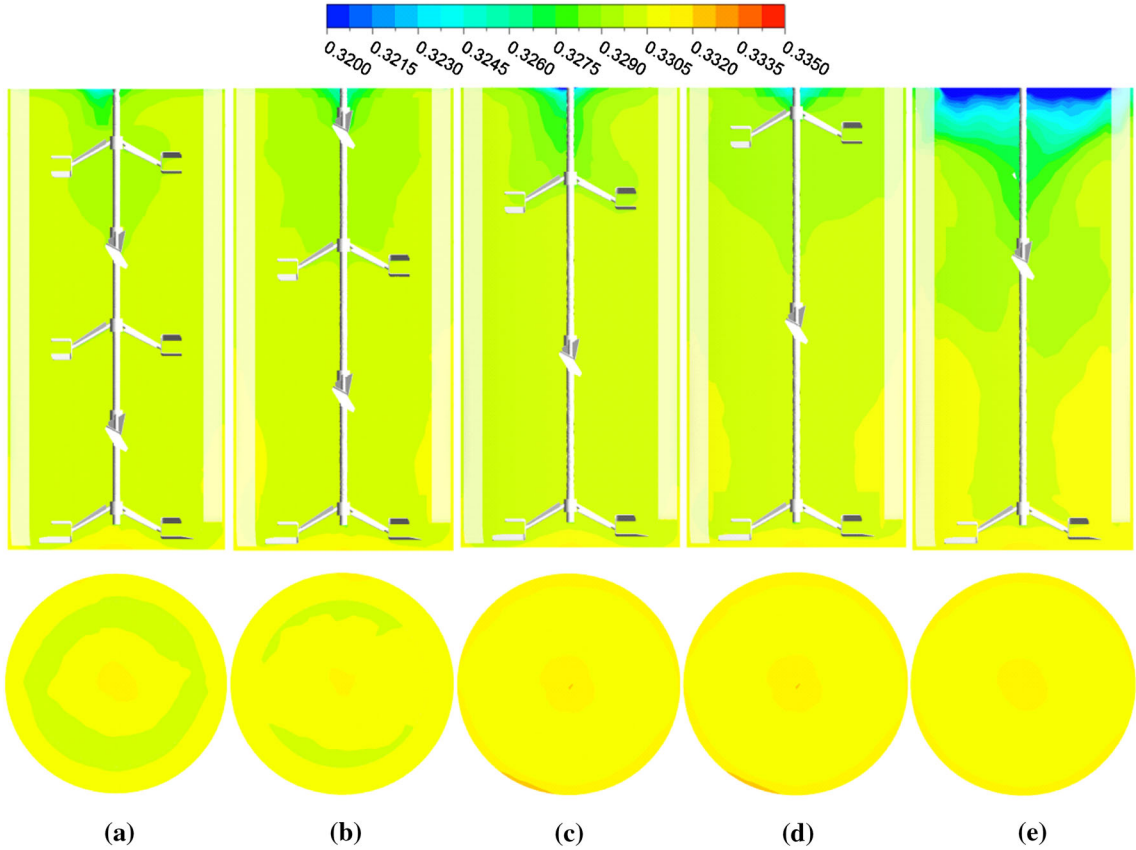

Fig. 9. Solid holdup distribution with different L/D at $Y = 0$ and $Z = 0$ sections (color map shows solids volume fraction): (a) five-stage ($L/D = 0.7$), (b) four-stage ($L/D = 1$), (c) three-stage ($L/D = 1.25$), (d) three-stage ($L/D = 1.5$), and (e) two-stage ($L/D = 2$).

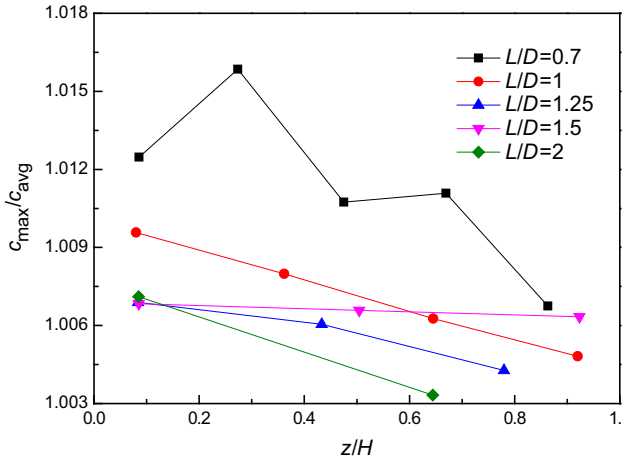

Fig. 10. Maximum of solids hold-up in the rotational region with different L/D.

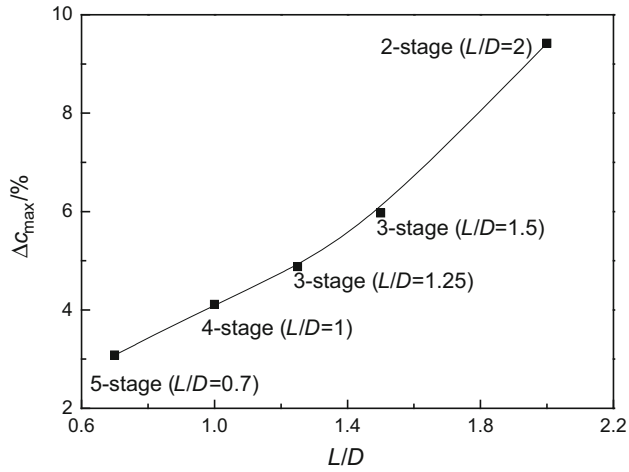

Fig. 11. Δc_{max} with different L/D.

Figures 13 and 14 show the total and average power consumption with different L/D. The power consumption depends on the number of impeller, the total power increases and the average power decreases with the increase of L/D. The total power with five-stage impellers is 67.2 kW, whereas it only 51.2 kW with three-stage impellers. Considering both mixing performance and power consumption, a three-stage impeller with L/D of 1.25 can meet the industrial requirements; moreover, more than 20% power could be saved compared with the current process conditions.

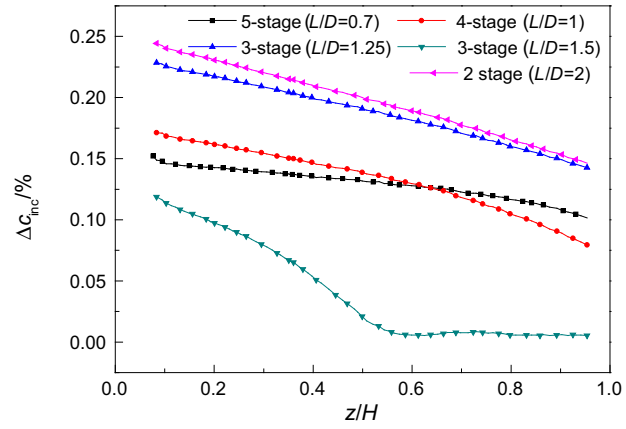

Fig. 12. Δc_{inc} distribution in the feed pipe with different L/D.

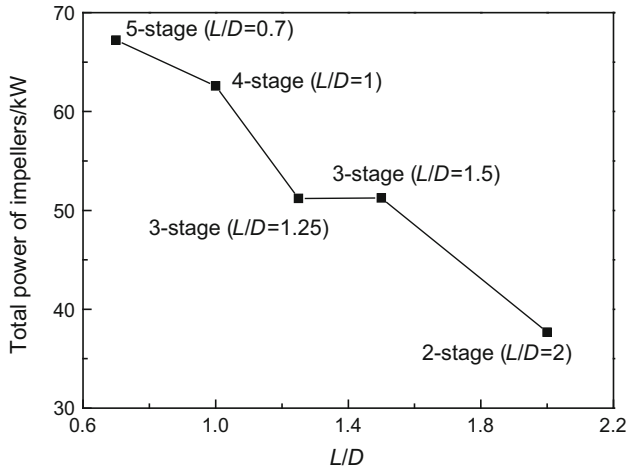

Fig. 13. Total power with different L/D.

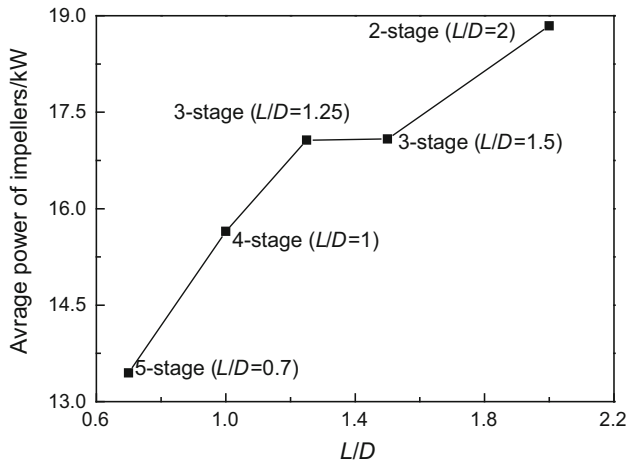

Fig. 14. Average power with different L/D.

CONCLUSION

1. The five-stage Intermig impellers coupled with sloped baffles can generate strong axial circulation loops, which is good for uniform solid mixing. With an increase of L/D, the circulation loop becomes weaker, and it is entirely isolated when $L/D \geq 1.5$.
2. The fluid, especially on the tank bottom, is overmixed under current industrial conditions. Increasing the separation distance between the impellers is good for uniform mixing in the rotational region.
3. The maximum concentration difference in the entire tank can be maintained at a level of less than 5% under the condition of the value of L/D is less than 1.25. The concentration increment in the feed pipe is less than 0.6% in all the five cases studied in this work.
4. Adopting a three-stage impeller with L/D of 1.25 can meet the industrial requirements; meanwhile, more than 20% power can be saved compared with the current process conditions.

ACKNOWLEDGEMENTS

This research was supported by the National Natural Science Foundation of China (No. 50974035 and No. 51074047) and the High Technology Research and Development Program of China (2010AA03A405).

REFERENCES

1. T.S. Zhang, C. Zhang, Y.C. Wang, Y.M. Dong, D.R. Zhang, Chinese Patent ZL200710158974.2 (2007).
2. N. Dohi, Y. Matsuda, N. Itano, K. Minekawa, T. Takahashi, and Y. Kawase, *Can. J. Chem. Eng.* 79, 107 (2001).
3. F. Magelli, D. Fajner, M. Nocentini, and G. Pasquali, *Chem. Eng. Sci.* 45, 615 (1990).
4. G.R. Kasat and A.B. Pandit, *Can. J. Chem. Eng.* 82, 892 (2004).
5. J. Aubin and C. Xuereb, *Chem. Eng. Sci.* 61, 2913 (2006).
6. T.A. Zhang, Y. Liu, S.C. Wang, H.L. Zhao, C. Zhang, Q.Y. Zhao, G.Z. Lv, and Z.H. Dou, *Light Metals 2011* (New York: TMS, 2011), p. 145.
7. Y. Liu, H.L. Zhao, T.A. Zhang, Q.Y. Zhao, S.C. Wang, S.Q. Gu, J.C. He, and C. Zhang, *Light Metals 2012* (New York: TMS, 2012), p. 113.
8. A.R. Khopkar, G.R. Kasat, A.B. Pandit, and V.V. Ranade, *Ind. Eng. Chem. Res.* 45, 4416 (2006).
9. J. Chen and W.D. Xiao, *Int. J. Chem. React. Eng.* 11, 331 (2013).
10. A. Ochieng and M.S. Onyango, *Powder Technol.* 181, 1 (2008).
11. C. Ford, F. Ein-Mozaffari, C.P.J. Bennington, and F. Taghipour, *AIChE J.* 52, 3562 (2006).
12. X.G. Shan, G.Z. Yu, C. Yang, Z.S. Mao, and W.G. Zhang, *Ind. Eng. Chem. Res.* 47, 2926 (2008).